Cancer Science

WILEY

Cancer Science

ORIGINAL ARTICLE OPEN ACCESS

Design and Evaluation of $Eb_4Mab\text{-}7\text{-}mG_{2a}$: A Dual-Action Anti-EphB4 Monoclonal Antibody for Targeted Breast Cancer Therapy

Tomokazu Ohishi[1] | Hiroyuki Suzuki[2] | Mika K. Kaneko[2] | Tomohiro Tanaka[2] | Akiko Harakawa[3] | Junjiro Yoshida[1] | Daisuke Tatsuda[1] | Yukinari Kato[2] | Manabu Kawada[1]

[1]Institute of Microbial Chemistry (BIKAKEN), Laboratory of Oncology, Microbial Chemistry Research Foundation, Tokyo, Japan | [2]Department of Antibody Drug Development, Tohoku University Graduate School of Medicine, Sendai, Miyagi, Japan | [3]Institute of Microbial Chemistry (BIKAKEN), Numazu, Microbial Chemistry Research Foundation, Shizuoka, Japan

Correspondence: Tomokazu Ohishi (ohishit@bikaken.or.jp) | Yukinari Kato (yukinari.kato.e6@tohoku.ac.jp)

Received: 26 June 2025 | **Revised:** 15 August 2025 | **Accepted:** 8 September 2025

Funding: This study was supported in part by the Japan Agency for Medical Research and Development (AMED) under grant numbers JP25am0521010, JP25ama121008, JP25ama221339, JP25bm1123027, and JP24ck0106730 (to Y.K.), and by the Japan Society for the Promotion of Science (JSPS) Grants-in-Aid for Scientific Research (KAKENHI) under grant numbers 22K06783 (to T.O.), 24K18268 (to T.T.), and 25K10553 (to Y.K.).

Keywords: antibody-dependent cellular cytotoxicity (ADCC) | breast cancer | complement-dependent cytotoxicity (CDC) | EphB4 | ligand blockade

ABSTRACT

Breast cancer remains a leading cause of cancer mortality worldwide, underscoring the urgent need for novel and effective therapeutic strategies. Eph receptor tyrosine kinases, particularly EphB4, exhibit diverse roles in cancer biology, acting as either tumor promoters or suppressors depending on the cellular environment and ligand engagement. EphB4 is frequently overexpressed in breast cancer and contributes to dysregulated signaling and tumor progression through the abnormal interaction with its ligand Ephrin-B2. We herein developed an improved anti-EphB4 monoclonal antibody, $Eb_4Mab\text{-}7\text{-}mG_{2a}$, which can be characterized as a subclass-switched IgG_{2a} variant designed to enhance immune effector function, specifically antibody-dependent cellular cytotoxicity (ADCC) and complement-dependent cytotoxicity (CDC). Our findings showed that $Eb_4Mab\text{-}7\text{-}mG_{2a}$ effectively blocked Ephrin-B2-induced ERK phosphorylation and proliferation in EphB4-positive MCF-7 breast cancer cells but had no effect on EphB4-knockout (KO) MCF-7 cells. Flow cytometry confirmed high-affinity binding between $Eb_4Mab\text{-}7\text{-}mG_{2a}$ and EphB4-expressing cells, whereas in vitro assays demonstrated potent and selective ADCC and CDC activities against EphB4-positive tumor cells. In vivo experiments showed that $Eb_4Mab\text{-}7\text{-}mG_{2a}$ significantly suppressed xenograft growth in models bearing EphB4-overexpressing CHO-K1 and EphB4-positive MCF-7, but showed no therapeutic effect in EphB4-negative CHO-K1 and EphB4-KO MCF-7 xenografts. Immunohistochemical analysis revealed reduced Ki-67 proliferation indices in treated tumors, supporting the antiproliferative effects of the developed antibody. Overall, these findings demonstrate that $Eb_4Mab\text{-}7\text{-}mG_{2a}$ exerts dual-action antitumor activity through ligand blockade and immune effector engagement. Further evaluations in other EphB4-overexpressing cancers and in combination with immune checkpoint inhibitors are warranted. Humanization and tumor-selective engineering may enhance its clinical potential for precision oncology.

Abbreviations: ADCC, antibody-dependent cellular cytotoxicity; CAR, chimeric antigen receptor; CasMab, cancer-specific monoclonal antibody; CDC, complement-dependent cytotoxicity; EphB4, erythropoietin-producing hepatocellular carcinoma receptor B4; ERK, extracellular signal-regulated kinase; FBS, fetal bovine serum; KO, knockout; mAb, monoclonal antibody; PBS, phosphate-buffered saline; PDPN, podoplanin; SDS–PAGE, sodium dodecyl sulfate–polyacrylamide gel electrophoresis; TME, tumor microenvironment.

1 | Introduction

Breast cancer remains one of the most common and lethal malignancies affecting women worldwide, accounting for 11.7% of all cancer cases and 6.9% of cancer-related deaths globally in 2020 [1]. Despite improvements in early detection and systemic therapies, breast cancer continues to be the second leading cause of cancer-related death among women [2], highlighting the urgent need for novel and more effective therapeutic strategies.

Eph receptor tyrosine kinases, which can be divided into EphA and EphB subclasses based on their ligand binding specificities, represent the largest family of receptor tyrosine kinases [3, 4]. EphB receptors, including EphB4, initiate downstream signaling by interacting with transmembrane Ephrin-B ligands. Among the EphB receptors, EphB4 has gained significant interest owing to its context-dependent roles in cancer biology, specifically its ability to act as either a tumor promoter or suppressor depending on the cellular environment and ligand availability [5].

EphB4 is frequently overexpressed in breast cancer and causes aberrant downstream signaling through its often dysregulated interaction with Ephrin-B2 [6]. This aberrant signaling promotes not only tumor proliferation but also angiogenesis and vascular remodeling in certain tumor contexts [5]. This dysregulation may be attributed to not only altered ligand availability but also changes in receptor localization or clustering, collectively enhancing ligand-dependent signaling through autocrine or paracrine mechanisms [5, 7]. Notably, Xiao et al. demonstrated that stimulating EphB4 with Ephrin-B2 or an agonistic monoclonal antibody in MCF-7 breast cancer cells activates the RAS/MEK/ERK signaling cascade, triggering enhanced cell proliferation [8]. In contrast, the same EphB4 activation in endothelial cells suppressed ERK activity and inhibited proliferation, illustrating the striking context-dependent function of EphB4 [9]. These mechanistic insights highlight the biological complexity of EphB4 and its significance as a context-specific therapeutic target. Altogether, these findings suggest that aberrant ligand-mediated EphB4 signaling, sustained even under partial ligand dysregulation, may drive malignant phenotypes via ERK pathway activation. Despite its context-dependent dual functionality, EphB4 can serve as a potential oncogenic driver in this setting.

Given the oncogenic potential of ligand-induced EphB4 signaling in breast cancer cells, blocking this pathway represents a promising therapeutic approach. In our previous work, we developed a monoclonal antibody, B4Mab-7 (also known as Eb_4Mab-7, IgG_1 kappa), that targets EphB4 [10]. In the present study, we engineered an improved version of this antibody, Eb_4Mab-7-mG_{2a}, which is a subclass-switched IgG_{2a} variant designed to enhance immune effector functions, such as antibody-dependent cellular cytotoxicity (ADCC) and complement-dependent cytotoxicity (CDC). This antibody exhibits dual functionality by simultaneously blocking Ephrin-B2-induced ERK signaling and activating immune effector mechanisms. Although several therapeutic antibodies function through either signaling modulation or immune-mediated cytotoxicity, studies have suggested that combining both mechanisms in a single antibody can enhance antitumor efficacy [11, 12].

As such, the current study aimed to evaluate the utility of Eb_4Mab-7-mG_{2a} as a novel bifunctional therapeutic candidate for EphB4-positive breast cancer by characterizing its mechanism of action and demonstrating its antitumor efficacy both in vitro and in vivo.

2 | Materials and Methods

2.1 | Kaplan–Meier Survival Analysis

Kaplan–Meier survival analysis was performed for all members of the EPHB gene families using the KMplot online tool (https://kmplot.com/analysis/), applying RNA-seq-based expression data from breast cancer samples. Overall survival (OS) was selected as the endpoint, with a follow-up threshold set at 120 months and censoring applied for data after such time point. Patients were divided into high and low expression groups using an automatically selected cutoff chosen from within the interquartile range to best separate survival outcomes. All other clinical and immune-related covariates were left unrestricted. Summary results, which include sample size (n), cutoff values, expression ranges, log-rank *P* values, false discovery rates (FDR), and hazard ratios (HRs), are presented in Table S1, with HRs and log-rank *P* values also shown in Figure 1A.

2.2 | Cell Lines and Cell Culture

Chinese hamster ovary (CHO)-K1, MCF-7, BT-474, SK-BR-3, MDA-MB-468, and MCF10A cell lines were obtained from the American Type Culture Collection (ATCC; Manassas, VA, USA). The HBC5 cell line was provided by the JCRB Cell Bank (Osaka, Japan). EphB4-overexpressing CHO-K1 (CHO/EphB4) and EphB4-knock out (KO) MCF-7 (also known as BINDS-52) cell lines were created in our previous study [10]. CHO-K1, HBC5, and CHO/EphB4 cells were cultured in Roswell Park Memorial Institute (RPMI)-1640 medium (Nacalai Tesque Inc., Kyoto, Japan) supplemented with 10% heat-inactivated fetal bovine serum (FBS; Thermo Fisher Scientific Inc., Waltham, MA, USA), 100 U/mL penicillin, 100 μg/mL streptomycin, and 0.25 μg/mL amphotericin B (Nacalai Tesque Inc.). MCF-7, BT-474, SK-BR-3, MDA-MB-468, and EphB4-KO MCF-7 cells were cultured in Dulbecco's Modified Eagle's Medium (DMEM; Nacalai Tesque Inc.) supplemented with 10% heat-inactivated FBS and the same antibiotics enumerated earlier. MCF10A cells were maintained in Mammary Epithelial Cell Growth Medium (Lonza, Walkersville, MD, USA) supplemented with growth supplements according to the manufacturer's instructions. All cells were incubated at 37°C in a humidified atmosphere containing 5% CO_2.

2.3 | Recombinant Antibody Production

Anti-EphB4 monoclonal antibody B4Mab-7 (IgG_1) was developed as previously described [10]. To produce recombinant

antibodies of the mouse IgG_1 and IgG_{2a} subclasses, V_H and V_L cDNA were isolated from hybridomas producing B4Mab-7. V_H cDNAs were combined with the C_H of mouse IgG_1 or IgG_{2a} and inserted into the pCAG-Ble vector (FUJIFILM Wako Pure Chemical Corporation, Osaka, Japan). Similarly, V_L cDNA and mouse kappa light chain were inserted into the pCAG-Neo vector (FUJIFILM Wako Pure Chemical Corporation). These vectors were then introduced into ExpiCHO or BINDS-09 cells (Fut8-KO ExpiCHO-S cells) using the ExpiCHO Expression System (Thermo Fisher Scientific Inc.) [13], after which the culture supernatants were harvested. B4Mab-7 and Eb_4Mab-7-mG_{2a} antibodies were purified using Ab-Capcher (ProteNova Co. Ltd., Kagawa, Japan).

2.4 | Western Blot Analysis

Western blot analysis was performed as described previously [14]. Cells were lysed using a buffer containing 20 mmol/L HEPES (pH 7.5), 150 mmol/L NaCl, 1% (v/v) Triton X-100, 10% (v/v) glycerol, 1 mmol/L EDTA, 50 mmol/L NaF, 50 mmol/L β-glycerophosphate, 1 mmol/L sodium orthovanadate (Na_3VO_4), and 25 μg/mL each of antipain, leupeptin, and pepstatin. For ERK phosphorylation analysis, MCF-7 and EphB4-KO MCF-7 cells were serum-starved for 12 h and then stimulated in 1% dialyzed FBS-containing medium with 5 μg/mL of recombinant human Ephrin-B2 (R&D Systems, Minneapolis, MN, USA) for 0, 5, 10, 15, 30, or 60 min. Cells were co-treated with 5 μg/mL Eb_4Mab-7-mG_{2a} or the control PMab-231 for the indicated durations at 37°C. PMab-231 is a mouse IgG_{2a} monoclonal antibody recognizing tiger podoplanin (PDPN) that does not cross-react with human cells and was used as a control antibody as previously reported [15]. Protein samples were separated by SDS-PAGE, transferred to polyvinylidene difluoride (PVDF) membranes, and immunoblotted with the primary antibodies listed later. Aside from cell lysates, a commercially available normal human breast tissue lysate (Total Protein–Human Adult Normal Tissue: Breast, Novus Biologicals, Littleton, CO, USA) was used to assess expression in normal breast tissue. Antibody binding was detected using appropriate horseradish peroxidase (HRP)-conjugated secondary antibodies (Cell Signaling Technology Inc., Danvers, MA, USA), followed by ECL detection (ECL Prime; Cytiva, Tokyo, Japan). The primary antibodies used were as follows: anti-phospho-ERK1/2 (Thr202/Tyr204; #4370, Cell Signaling Technology Inc.), anti-total ERK1/2 (clone C-9; sc-514302, Santa Cruz Biotechnology, Dallas, TX, USA), anti-EphB4 (Eb_4Mab-7-mG_{2a}), anti-β-actin (D6A8) Rabbit mAb (HRP Conjugate; #12620, Cell Signaling Technology Inc.), and anti-GAPDH (D16H11) XP Rabbit mAb (#5174, Cell Signaling Technology Inc.). Band intensities were quantified using ImageJ software.

2.5 | Proliferation Assay In Vitro

Cell proliferation was evaluated using the MTS tetrazolium assay (CellTiter 96 Aqueous One Solution Cell Proliferation Assay; Promega, Madison, WI, USA). Cells were plated into 96-well plates at 2000 cells per well in 100 μL of medium containing test agents such as antibodies or recombinant Ephrin-B2. At the indicated time points (typically 0 to 3 days), 20 μL of MTS reagent was added directly to each well (final volume 120 μL) and incubated for 30 min at 37°C. Absorbance was measured at 490 nm with a reference wavelength of 630 nm using a PowerScan HT microplate reader (BioTek Instruments, Winooski, VT, USA). Triplicate wells were analyzed for each condition, with the results being expressed as mean ± standard deviation (SD). Statistical significance was determined using the Mann–Whitney *U* test. $*p < 0.05$; $**p < 0.01$; n.s., not significant.

2.6 | Flow Cytometry

The CHO-K1, CHO/EphB4, MCF-7, and EphB4-KO MCF-7 cell lines were harvested using 1 mM ethylenediaminetetraacetic acid (EDTA; Nacalai Tesque Inc.) combined with 0.25% trypsin. Cells were incubated with B4Mab-7, Eb_4Mab-7-mG_{2a}, or a control blocking buffer (0.1% bovine serum albumin (BSA) in phosphate-buffered saline (PBS)) for 30 min at 4°C, followed by Alexa Fluor 488-conjugated anti-mouse IgG (1:2000; Cell Signaling Technology Inc.) for an additional 30 min. Fluorescence data were acquired using the SA3800 Cell Analyzer (Sony Corp., Tokyo, Japan) and analyzed using SA3800 software version 2.05 (Sony Corp.).

2.7 | Determination of the Dissociation Constant (K_D) via Flow Cytometry

To determine the K_D, CHO/EphB4 and MCF-7 cells were resuspended in 100 μL of Eb_4Mab-7-mG_{2a} at concentrations ranging from 0.001 to 20 μg/mL in a 1:2 serial dilutions in the blocking buffer and incubated for 30 min. After washing twice with 0.1% BSA in PBS, 50 μL of Alexa Fluor 488-conjugated anti-mouse IgG (1:200; Cell Signaling Technology Inc.) was added, followed by a 30-min incubation. Following the incubation, the cells were washed twice and plated into a 96-well plate for measurement. Fluorescence data were acquired using the SA3800 Cell Analyzer and processed using FlowJo software. The K_D was determined by fitting the binding isotherms to a one-site binding model using GraphPad Prism 6 (GraphPad Software Inc., La Jolla, CA, USA).

2.8 | ADCC

The ADCC assay was performed following previously published methods [16]. Briefly, 12 female BALB/c nude mice (5 weeks old) were purchased from The Jackson Laboratory Inc. (Kanagawa, Japan). After removing the spleens, single-cell suspensions were prepared by passing the spleen tissue through a sterile cell strainer (catalog number 352360; Falcon, BD Biosciences, Franklin Lakes, NJ, USA). To eliminate erythrocytes, the splenocytes were lysed with ice-cold distilled water for 30 s, followed by immediate neutralization with isotonic buffer. The remaining splenocytes were then resuspended in RPMI or DMEM supplemented with 10% FBS, forming the effector cell preparation. Target cells (CHO-K1, CHO/EphB4, MCF-7, or EphB4-KO MCF-7) were labeled with 10 μg/mL calcein AM (Thermo Fisher Scientific Inc.) and resuspended in the same medium. Target cells (1×10^4 per well) were plated into 96-well plates, combined with effector cells

at a ratio of 50:1, and treated with 100 μg/mL of Eb_4Mab-7-mG_{2a} or control PMab-231. After incubation at 37°C for 4.5 h, the amount of calcein released into the supernatant was measured. Fluorescence intensity was detected using a microplate reader (PowerScan HT; BioTek Instruments Inc., Winooski, VT, USA) with excitation and emission wavelengths of 485 and 538 nm, respectively. The percentage of lysis was calculated using the following formula: (fluorescence from target-effector cultures−spontaneous fluorescence of the target cells alone)/(maximum fluorescence after complete lysis−spontaneous fluorescence) × 100. Complete cell lysis was achieved using a buffer containing 0.5% Triton X-100, 10 mM Tris–HCl (pH 7.4), and 10 mM EDTA. All experiments were conducted in triplicate.

2.9 | CDC

The CDC assay was performed following established procedures [16]. Briefly, the cells were labeled with 10 μg/mL calcein AM, suspended in the medium, and plated into 96-well plates at 1×10^4 cells per well. Rabbit complement (final dilution 1:10; Low-Tox-M Rabbit Complement; Cedarlane Laboratories, Hornby, ON, Canada) and 100 μg/mL of Eb_4Mab-7-mG_{2a} or control PMab-231 were added to the wells. After 4.5 h of incubation at 37°C, calcein released into the supernatant was measured, and fluorescence intensity was calculated as described in the ADCC section.

2.10 | Antitumor Activity In Vivo

All procedures involving animals were conducted in accordance with institutional guidelines and received approval from the Animal Ethics Committee of the Institute of Microbial Chemistry (Numazu, Japan; approval number 2024–071). Female BALB/c nude mice (5 weeks old) were obtained from The Jackson Laboratory Inc. and maintained under pathogen-free conditions. Subcutaneous xenografts were created by injecting 5×10^6 CHO-K1, CHO/EphB4, MCF-7, or EphB4-KO MCF-7 cells mixed with Matrigel (BD Biosciences) into the left flank of each mouse. Antibodies (Eb_4Mab-7-mG_{2a} or control PMab-231) were then delivered intraperitoneally at a dosage of 100 μg per mouse on Days 7, 14, and 21 following cell inoculation. Thereafter, tumor volumes were measured twice a week using calipers and calculated by multiplying the square of the shorter diameter by the longer diameter and dividing the result by two.

2.11 | Immunohistochemical Analysis

Immunohistochemical analysis of mouse xenograft tumor tissues was performed as previously described [14]. Briefly, paraffin-embedded tissue sections were cut and mounted on microscope slides. After deparaffinization with xylene and rehydration through a graded ethanol series, endogenous peroxidase activity was blocked with methanol containing hydrogen peroxide. Antigen retrieval was performed by boiling the sections in 0.01 M sodium citrate buffer (pH 6.0) for 10 min. The sections were then incubated for 60 min at room temperature with an anti-Ki-67 antibody (1:200 dilution; clone SP6, ab16667, Abcam, Cambridge, United Kingdom). Immunoreactivity was visualized using 3,3′-diaminobenzidine with the ChemMate EnVision kit (Dako, Carpinteria, CA, USA), followed by counterstaining with hematoxylin. Stained sections were examined under a Nikon Biophot microscope (Nikon, Tokyo, Japan), and images were captured with an ECLIPSE TE2000-U microscope (Nikon). Ki-67-positive cells were quantified using e-Path image analysis software (e-Path Co., Tokyo, Japan).

2.12 | Statistical Analysis

All experiments were conducted in triplicate, with data being expressed as the mean ± SD. In most figures, error bars indicate mean ± SD. In some figures, SD is shown in the positive direction only, as noted in their corresponding legends. Statistical analyses were performed using either two-way ANOVA followed by Tukey's or Sidak's multiple comparison tests or the non-parametric Mann–Whitney U test, as appropriate. All analyses were conducted using GraphPad Prism 10 software (GraphPad Software Inc., La Jolla, CA, USA).

3 | Results

3.1 | Development of a Class-Switched Anti-EphB4 Monoclonal Antibody and Analysis of EphB4 Expression Across Breast Cancer Subtypes

To determine the clinical relevance of EphB4 expression in breast cancer, Kaplan–Meier survival analysis was first performed using RNA-seq-based datasets from KMplot. Among the EphB family members, high EphB4 expression was significantly associated with poor OS among breast cancer patients (Figure 1A), suggesting the potential oncogenic role of EphB4. High EphB2 expression was also significant, but subsequent analyses focused on EphB4 given its slightly higher hazard ratio and established relevance in breast cancer.

The mouse IgG_1 monoclonal antibody B4Mab-7, previously developed by our group, specifically recognizes EphB4-expressing tumor cells [10]. To enhance its effector functions, such as ADCC and CDC, B4Mab-7 was class-switched into mouse IgG_{2a} format, resulting in the generation of Eb_4Mab-7-mG_{2a} (Figure 1B). To examine EphB4 protein expression across cell models, Western blot analysis was performed using lysates from CHO-K1, CHO/EphB4, MCF-7, and EphB4-KO MCF-7 cells. Notably, we found that Eb_4Mab-7-mG_{2a} triggered an increase in the expression of EphB4 in CHO/EphB4 and MCF-7 cells but not in CHO-K1 and EphB4-KO MCF-7 cells (Figure 1C). Furthermore, EphB4 was expressed in multiple breast cancer cell lines representing different subtypes, including BT-474 (luminal B), SK-BR-3 (HER2+), MDA-MB-468 (basal-like), and HBC5 (triple-negative). However, EphB4 was barely detectable in MCF10A, a non-tumorigenic mammary epithelial cell line, and in lysates of normal human breast tissue (Figure 1C). Altogether, these findings indicate that EphB4 is frequently overexpressed across diverse breast cancer subtypes relative to normal breast tissue. This pattern of differential expression is further supported by previous clinical and transcriptomic studies. Kumar et al. found

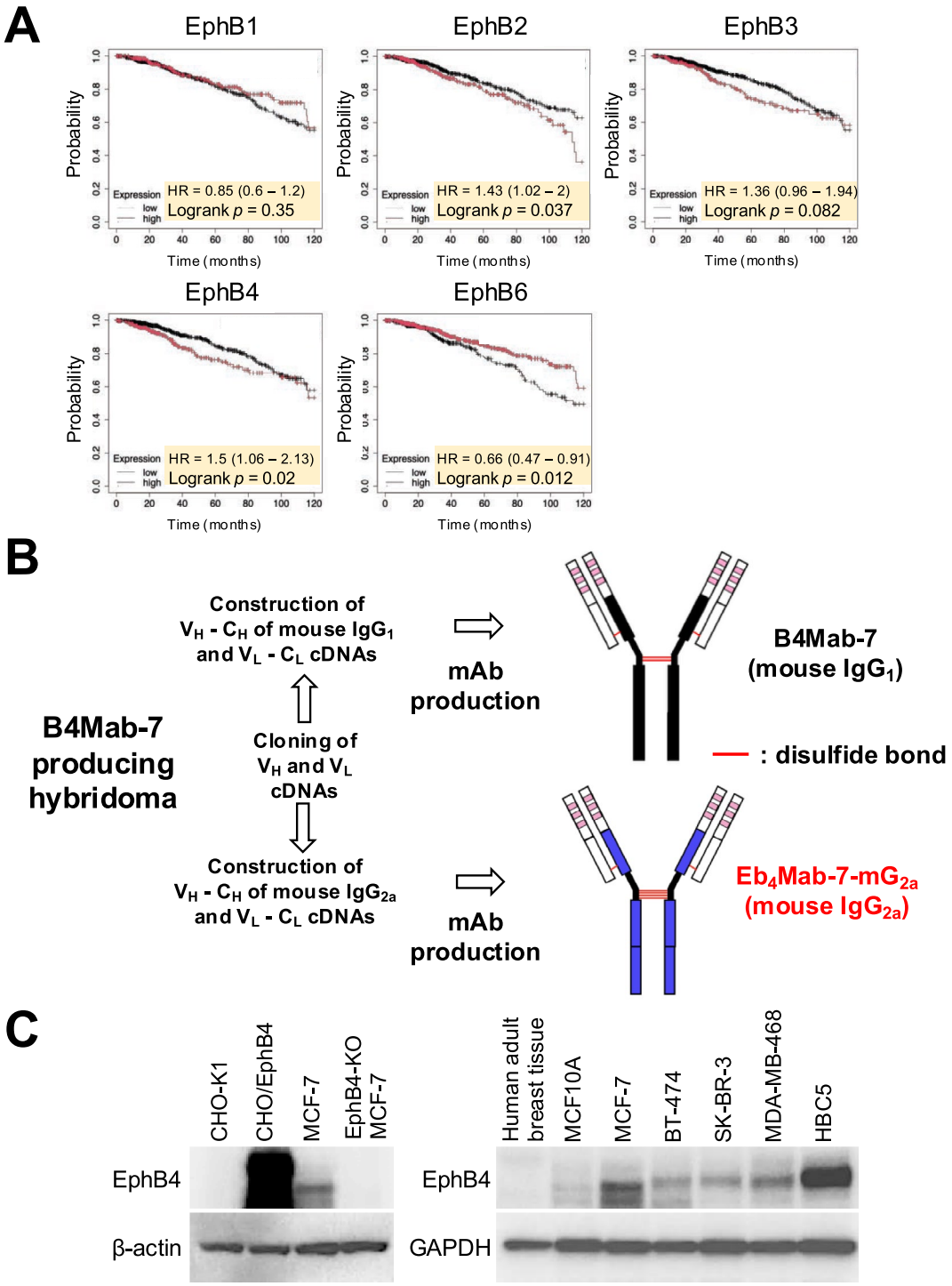

FIGURE 1 | Prognostic significance of EphB4 expression in breast cancer and establishment of Eb_4Mab-7-mG_{2a}. (A) Kaplan–Meier survival analysis of OS in breast cancer patients based on the expression levels of EphB family genes (EphB1, EphB2, EphB3, EphB4, and EphB6) using RNA-seq data from KMplot. Among these genes, high expression of EphB2 and EphB4 was significantly associated with poor prognosis (log-rank $p < 0.05$). Patients were then stratified into high and low expression groups using the optimal cutoff within the interquartile range. (B) Generation of a mouse IgG_{2a} version of the anti-EphB4 monoclonal antibody (Eb_4Mab-7-mG_{2a}). The V_H and V_L regions of B4Mab-7 (mouse IgG_1) were cloned into expression vectors containing mouse IgG_{2a} C_H and C_L regions. These vectors were transfected into BINDS-09 cells to produce Eb_4Mab-7-mG_{2a}. (C) Left: Expression of EphB4 and β-Actin in CHO-K1, CHO/EphB4, MCF-7, and EphB4-KO MCF-7 cells. Right: Expression of EphB4 and GAPDH in normal human adult breast tissues, MCF10A (non-tumorigenic mammary epithelial cells), MCF-7, BT-474, SK-BR-3, MDA-MB-468, and HBC5 cells.

that EphB4 is highly expressed in a large proportion of human breast tumors and functions as a survival factor [17]. Ding et al. further demonstrated that EphB4 expression is particularly elevated in HER2-positive breast cancers and is associated with poor clinical outcomes [18]. Supporting its prognostic relevance, Brantley-Sieders et al. reported that high EphB4 expression correlates with reduced OS and increased recurrence risk in breast cancer patients [19].

3.2 | Effect of Eb_4Mab-7-mG_{2a} on Ephrin-B2-Induced Cell Proliferation and ERK Signaling

Given that EphB4 is frequently overexpressed in breast cancer and associated with poor prognosis, we sought to determine whether EphB4 contributes functionally to tumor cell behavior upon ligand engagement. To this end, we examined the effects of Ephrin-B2, a known ligand of EphB4, on cell proliferation. Intriguingly, Ephrin-B2 stimulation promoted the proliferation of MCF-7 cells but not EphB4-negative MCF10A cells, indicating ligand-dependent proliferative signaling mediated by EphB4 (Figure 2A). However, co-treatment with Eb_4Mab-7-mG_{2a} significantly suppressed Ephrin-B2-induced proliferation in MCF-7 but not in MCF10A cells (Figure 2B). Furthermore, Ephrin-B2 stimulation promoted time-dependent ERK1/2 phosphorylation in MCF-7 cells, which was diminished by co-treatment with Eb_4Mab-7-mG_{2a} but not with control PMab-231 (Figure 2C). No such signaling was observed in EphB4-KO MCF-7 cells, confirming that EphB4 specifically activated the ERK pathway. These results suggest that Eb_4Mab-7-mG_{2a} inhibits Ephrin-B2-induced ERK signaling associated with proliferation in EphB4-expressing breast cancer cells.

In contrast, treatment with Eb_4Mab-7-mG_{2a} alone did not alter cell proliferation in MCF10A, MCF-7, or HBC5 cells across a 3-day culture period, suggesting minimal basal agonistic or toxic activity (Figure S1). Notably, although EphB4 displayed a relatively high endogenous expression in HBC5 cells, which represent a triple-negative breast cancer subtype, no growth-inhibitory effect was observed in the absence of Ephrin-B2 stimulation, further supporting the specificity and ligand-dependency of the antibody's action.

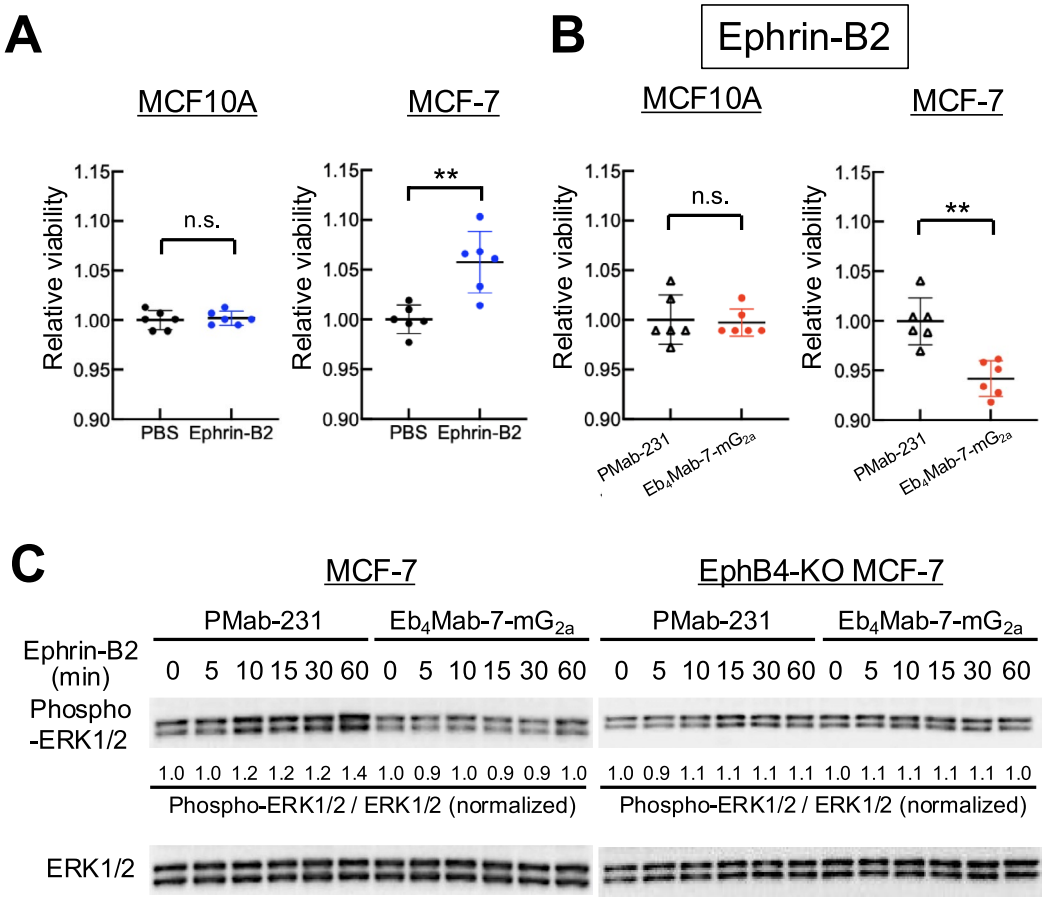

FIGURE 2 | Inhibitory effects of Eb_4Mab-7-mG_{2a} on Ephrin-B2-induced proliferation and ERK activation in EphB4-expressing breast cancer cells. (A) Viability of MCF10A and MCF-7 cells treated with recombinant Ephrin-B2 (5 μg/mL) or PBS for 3 days. Cell proliferation was assessed using the MTS assay and normalized to Day 0 (set as 1.0). Ephrin-B2 significantly enhanced the proliferation of MCF-7 cells but not MCF10A cells relative to PBS control. Values are expressed as mean ± SD ($n = 6$). Asterisks indicate statistical significance (**$p < 0.01$; n.s., not significant; Mann–Whitney U test). (B) Viability of MCF10A and MCF-7 cells treated with recombinant Ephrin-B2 (5 μg/mL) in the presence of control PMab-231 or anti-EphB4 antibody (Eb_4Mab-7-mG_{2a}, 5 μg/mL) for 0 to 3 days. Cell proliferation was assessed using the MTS assay and normalized to Day 0 (set as 1.0). Eb_4Mab-7-mG_{2a} significantly suppressed Ephrin-B2-induced proliferation of MCF-7 cells, whereas no significant effect was observed in MCF10A cells. Values are expressed as mean ± SD ($n = 6$). Asterisks indicate statistical significance (**$p < 0.01$; n.s., not significant; Mann–Whitney U test). (C) Activation of ERK signaling in MCF-7 and EphB4-KO MCF-7 cells after stimulation with recombinant Ephrin-B2 (5 μg/mL) for the indicated time points (0–60 min). Cells were pretreated with either control PMab-231 or Eb_4Mab-7-mG_{2a} (5 μg/mL) prior to stimulation. ERK1/2 phosphorylation was analyzed using Western blot analysis with anti-phospho-ERK1/2 and total ERK1/2 antibodies. Ephrin-B2 stimulation increased ERK1/2 phosphorylation in parental MCF-7 cells, which was attenuated by Eb_4Mab-7-mG_{2a}. No phosphorylation was observed in EphB4-KO MCF-7 cells. Band intensities were quantified using ImageJ. Phospho-ERK1/2 / ERK1/2 ratios normalized to the 0 min time point are shown below each band.

3.3 | Binding Activity of Eb_4Mab-7-mG_{2a} and B4Mab-7 Against EphB4-Expressing and Control Cells

Both Eb_4Mab-7-mG_{2a} and its parental antibody B4Mab-7 exhibited dose-dependent binding to CHO/EphB4 and MCF-7 cells, as assessed by flow cytometry using increasing antibody concentrations (0.01–10 μg/mL) (Figure 3). In contrast, neither antibody showed detectable binding to EphB4-negative CHO-K1 or EphB4-KO MCF-7 cells (Figure 3). These results confirm the high specificity of both antibodies for human EphB4 and demonstrate that class switching to IgG_{2a} preserves target recognition.

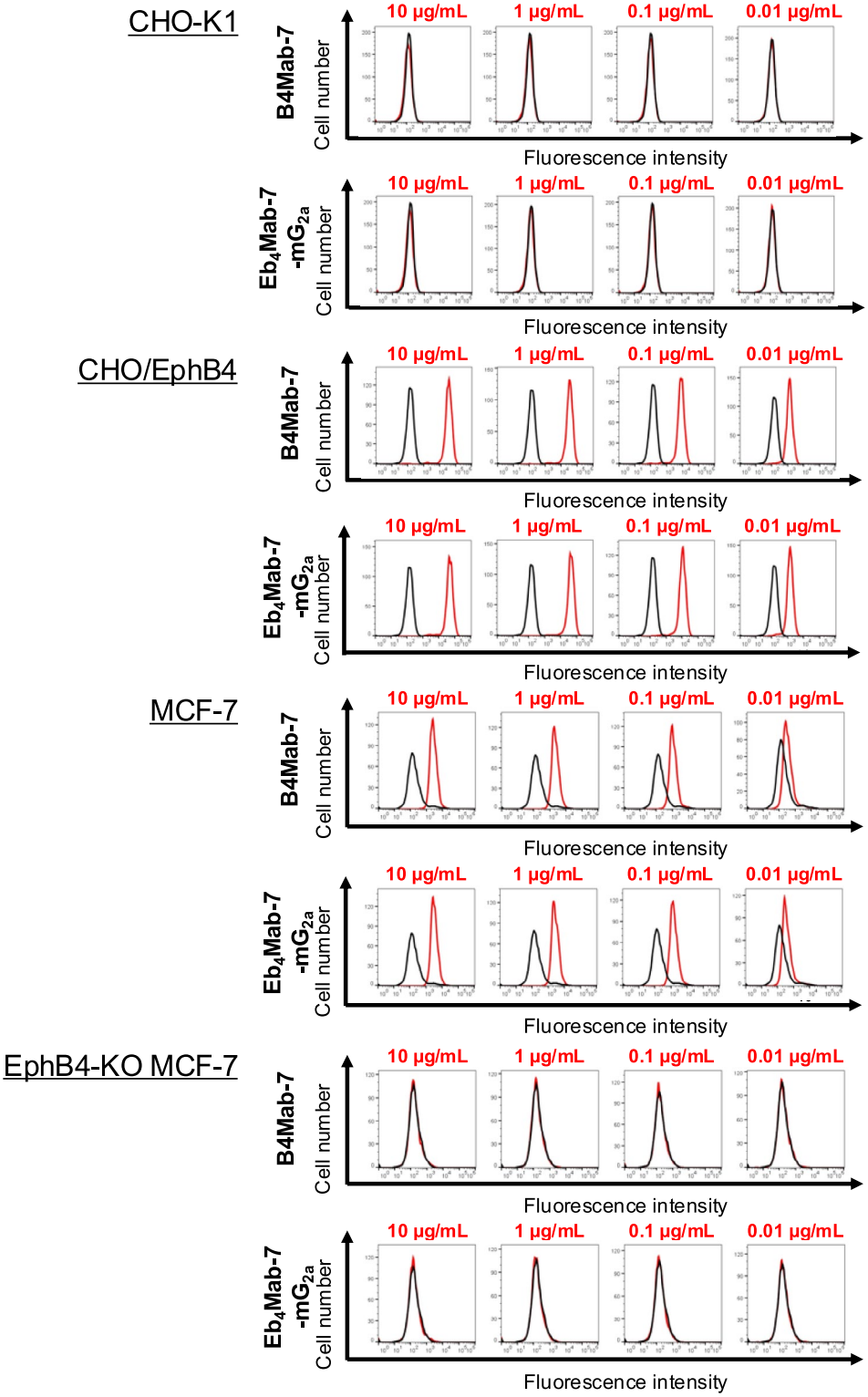

FIGURE 3 | Flow cytometry analysis of EphB4 binding to B4Mab-7 and Eb_4Mab-7-mG_{2a}. CHO-K1, CHO/EphB4, MCF-7, and EphB4-KO MCF-7 cells were incubated with buffer (black histograms) or increasing concentrations (0.01–10 μg/mL) of B4Mab-7 or Eb_4Mab-7-mG_{2a} (red histograms), followed by Alexa Fluor 488-conjugated anti-mouse IgG. Fluorescence was then analyzed using the SA3800 Cell Analyzer.

3.4 | Binding Affinity of $Eb_4Mab\text{-}7\text{-}mG_{2a}$ for EphB4-Expressing Cells

Flow cytometry was used to perform a kinetic analysis of $Eb_4Mab\text{-}7\text{-}mG_{2a}$ binding to EphB4-expressing cells. As shown in Figure 4A,B, the K_D of $Eb_4Mab\text{-}7\text{-}mG_{2a}$ was 5.4×10^{-9} M for CHO/EphB4 cells and 8.5×10^{-10} M for MCF-7 cells, which endogenously express EphB4. These results indicate that $Eb_4Mab\text{-}7\text{-}mG_{2a}$ exhibits high binding affinity for both overexpressed and endogenous EphB4.

The affinity of $Eb_4Mab\text{-}7\text{-}mG_{2a}$ for MCF-7 cells was approximately 6.4-fold higher than that for CHO/EphB4 cells, which may reflect differences in the spatial distribution, glycosylation status, or the membrane environment of EphB4 between the two cell lines. Overall, these results highlight the suitability of

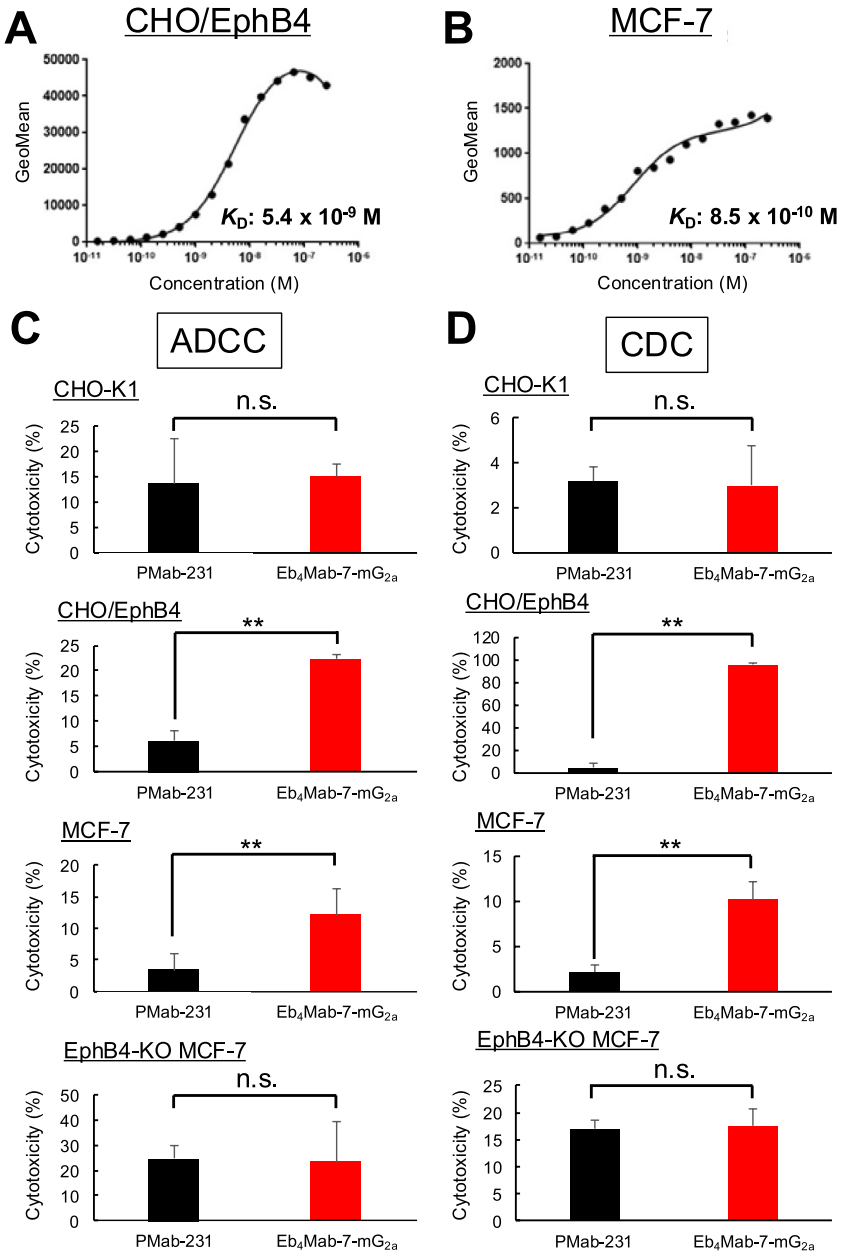

FIGURE 4 | Binding affinity and effector functions of $Eb_4Mab\text{-}7\text{-}mG_{2a}$. (A, B) Binding affinity of $Eb_4Mab\text{-}7\text{-}mG_{2a}$ to CHO/EphB4 (A) and MCF-7 (B) cells. Cells were incubated with serial dilutions of $Eb_4Mab\text{-}7\text{-}mG_{2a}$, followed by Alexa Fluor 488-conjugated anti-mouse IgG. Fluorescence intensity was analyzed using the SA3800 Cell Analyzer, while the K_D was calculated using GraphPad Prism. (C, D) ADCC and CDC of $Eb_4Mab\text{-}7\text{-}mG_{2a}$. Calcein-labeled CHO-K1, CHO/EphB4, MCF-7, and EphB4-KO MCF-7 cells were treated with $Eb_4Mab\text{-}7\text{-}mG_{2a}$ or a control PMab-231. For ADCC (C), effector splenocytes were added. For CDC (D), rabbit complement was used. Cytotoxicity was assessed by measuring calcein release into the medium. Data are presented as means ± SD shown in the positive direction only. Asterisks indicate statistical significance (**$p < 0.01$; n.s., not significant; one-way ANOVA with Tukey's multiple comparisons test).

Eb_4Mab-7-mG_{2a} for targeting EphB4-positive cells given its high binding affinity with them.

3.5 | Evaluating the ADCC and CDC Activities of Eb_4Mab-7-mG_{2a}

Eb_4Mab-7-mG_{2a} exhibited significant ADCC activity against EphB4-expressing CHO/EphB4 and MCF-7 cells compared to the control PMab-231 but demonstrated no ADCC activity against EphB4-negative CHO-K1 or EphB4-KO MCF-7 cells (Figure 4C). Similarly, CDC activity was observed in CHO/EphB4 and MCF-7 cells but not in CHO-K1 or EphB4-KO MCF-7 cells (Figure 4D). Overall, these results indicate that Eb_4Mab-7-mG_{2a} selectively mediates immune effector-driven cytotoxicity against EphB4-expressing cells, highlighting its therapeutic potential for targeting EphB4-positive tumors.

3.6 | Growth-Inhibitory Efficacy of Eb_4Mab-7-mG_{2a} in CHO-Derived Xenograft Models

To assess the in vivo therapeutic potential of Eb_4Mab-7-mG_{2a}, xenograft experiments were subsequently performed using the previously described CHO-K1, CHO/EphB4, MCF-7, and EphB4-KO MCF-7 cells. Antibodies were administered intraperitoneally once per week (100 μg/mouse) for a total of three injections.

Our results for the CHO-K1 xenograft model (Figure 5A–C and Figure S2A) found no significant differences in xenograft growth over time (Figure 5A), macroscopic appearance of resected xenografts (Figure 5B), xenograft weight upon sacrifice (Figure 5C), or body weight changes throughout the treatment period (Figure S2A, left) between mice treated with Eb_4Mab-7-mG_{2a} and those receiving control PMab-231. Representative images of mice upon sacrifice also showed no visible differences in xenograft burden between groups (Figure S2A, right). Furthermore, Ki-67 immunohistochemistry of xenograft sections revealed no significant difference in the proliferation index between the two treatment groups (Figure 7A,B), suggesting that Eb_4Mab-7-mG_{2a} displayed no growth-inhibitory effects against EphB4-negative cells.

In contrast, our results for the CHO/EphB4 xenograft model (Figure 5D–F, Figure S2B) found that treatment with Eb_4Mab-7-mG_{2a} significantly inhibited xenograft growth compared to control PMab-231, as evidenced by reductions in the xenograft volume over time (Figure 5D), size of the resected xenografts (Figure 5E), and xenograft weight at sacrifice (Figure 5F). No significant difference in body weight was observed between the two groups during the treatment period (Figure S2B, left), indicating that the antibody treatment was well tolerated. Representative images of the mice upon sacrifice also showed a visibly reduced xenograft burden in the Eb_4Mab-7-mG_{2a}-treated group (Figure S2B, right). Ki-67 immunohistochemistry further confirmed the growth-inhibitory effects of Eb_4Mab-7-mG_{2a}, which promoted a significant reduction in the proliferation index in xenografts derived from CHO/EphB4 cells compared to those treated with control antibody (Figure 7C,D). Overall, these results demonstrate that Eb_4Mab-7-mG_{2a} exerts a potent growth-inhibitory effect in vivo against EphB4-overexpressing xenografts by inhibiting cell proliferation.

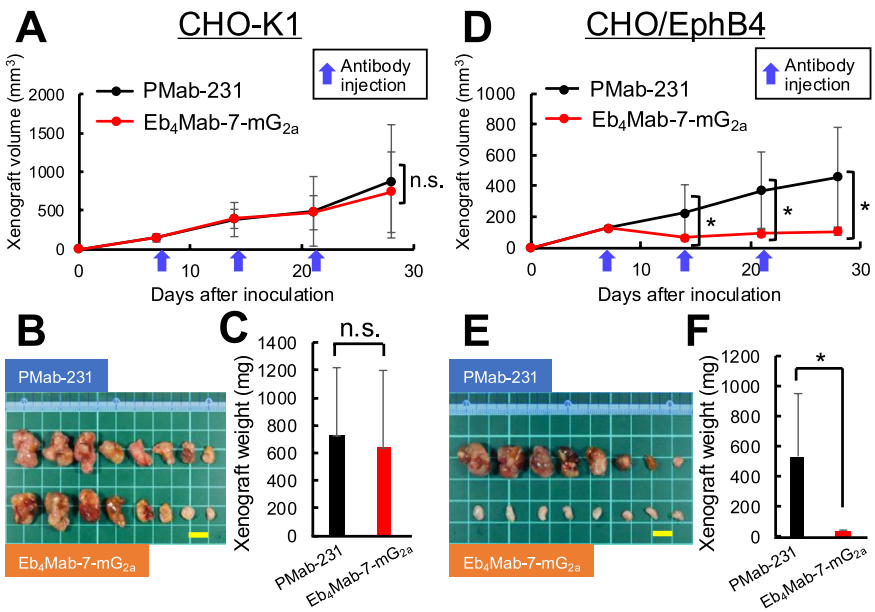

FIGURE 5 | Growth-inhibitory activity of Eb_4Mab-7-mG_{2a} against EphB4-overexpressing cells in vivo. CHO-K1 and CHO/EphB4 cells were subcutaneously inoculated into BALB/c nude mice on Day 0. Eb_4Mab-7-mG_{2a} (100 μg) or the control PMab-231 (100 μg) was administered intraperitoneally on Days 7, 14, and 21 (indicated by blue arrows). (A, D) Growth curves of CHO-K1 (A) and CHO/EphB4 (D) xenografts. Xenograft volumes are presented as mean ± SD. *$p < 0.05$ (two-way ANOVA with Sidak's multiple comparisons test). (B, E) Representative images of resected xenografts derived from CHO-K1 (B) and CHO/EphB4 (E) (scale bar: 1 cm). (C, F) Xenograft weights at the endpoint from CHO-K1 (C) and CHO/EphB4 (F). *$p < 0.05$ (two-way ANOVA with Sidak's multiple comparisons test).

3.7 | Antitumor Efficacy of $Eb_4Mab\text{-}7\text{-}mG_{2a}$ in MCF-7-Derived Xenograft Models

We subsequently examined the therapeutic efficacy of $Eb_4Mab\text{-}7\text{-}mG_{2a}$ in a clinically relevant model using MCF-7 breast cancer cells, which endogenously express EphB4 and EphB4-KO MCF-7 cells. The same dosing schedule, that is, intraperitoneal administration of antibody (100 μg/mouse) once per week for 3 weeks, was employed.

In the MCF-7 xenograft model (Figure 6A–C and Figure S3A), $Eb_4Mab\text{-}7\text{-}mG_{2a}$ significantly suppressed tumor growth compared to control PMab-231, as indicated by reductions in tumor volume over time (Figure 6A), tumor size upon resection (Figure 6B), and tumor weight upon sacrifice (Figure 6C). Body weight changes did not significantly differ between the two groups (Figure S3A, left), with the representative images upon sacrifice demonstrating a visible reduction in tumor size in the $Eb_4Mab\text{-}7\text{-}mG_{2a}$-treated group (Figure S3A, right). Consistent with these findings, Ki-67 staining of tumor sections showed significantly decreased proliferation in the treated group compared to controls (Figure 7E,F), supporting the antiproliferative effects of the antibody in EphB4-expressing breast cancer.

In contrast, no significant antitumor effects were observed in the EphB4-KO MCF-7 xenograft model (Figure 6D–F and Figure S3B). In particular, tumor volume (Figure 6D), macroscopic appearance (Figure 6E), tumor weight (Figure 6F), and body weight (Figure S3B, left) were all comparable between the $Eb_4Mab\text{-}7\text{-}mG_{2a}$ and control antibody groups. Additionally, no visible tumor regression was observed in mice (Figure S3B, right), with Ki-67 staining revealing no significant difference in proliferation index between groups (Figure 7G,H). These results confirm that the antitumor activity of $Eb_4Mab\text{-}7\text{-}mG_{2a}$ is dependent on EphB4 expression in vivo.

4 | Discussion

The current study demonstrated that $Eb_4Mab\text{-}7\text{-}mG_{2a}$, a subclass-switched anti-EphB4 monoclonal antibody, exerts potent antitumor activities against EphB4-positive breast cancer through two mechanisms, namely ligand blockade and immune effector activation. This antibody selectively inhibited Ephrin-B2-induced ERK phosphorylation and proliferation in EphB4-positive MCF-7 cells but exhibited no effect in EphB4-KO or ligand-unstimulated cells, highlighting its specificity (Figure 2). Consistent with these functional effects, flow cytometric analysis confirmed that both $Eb_4Mab\text{-}7\text{-}mG_{2a}$ and its parental IgG_1 antibody B4Mab-7 selectively bound to EphB4-expressing CHO/EphB4 and MCF-7 cells in a dose-dependent manner, but not to EphB4-negative CHO-K1 or EphB4-KO MCF-7 cells, supporting the specificity of antigen recognition (Figure 3). Moreover, subclass switching to IgG_{2a} enhanced ADCC and CDC activity against EphB4-positive tumor cells in vitro, with no cytotoxicity observed in EphB4-negative and EphB4-KO controls (Figures 2 and 4).

Importantly, although robust ADCC and CDC activities were demonstrated in vitro, it remains to be clarified whether these immune effector functions can be fully recapitulated within the tumor microenvironment (TME), which is often immunosuppressive and heterogeneous in immune cell composition [20]. The suppressive TME is characterized by the presence of regulatory T cells, myeloid-derived suppressor cells (MDSCs), and M2-like tumor-associated macrophages that inhibit NK cell or

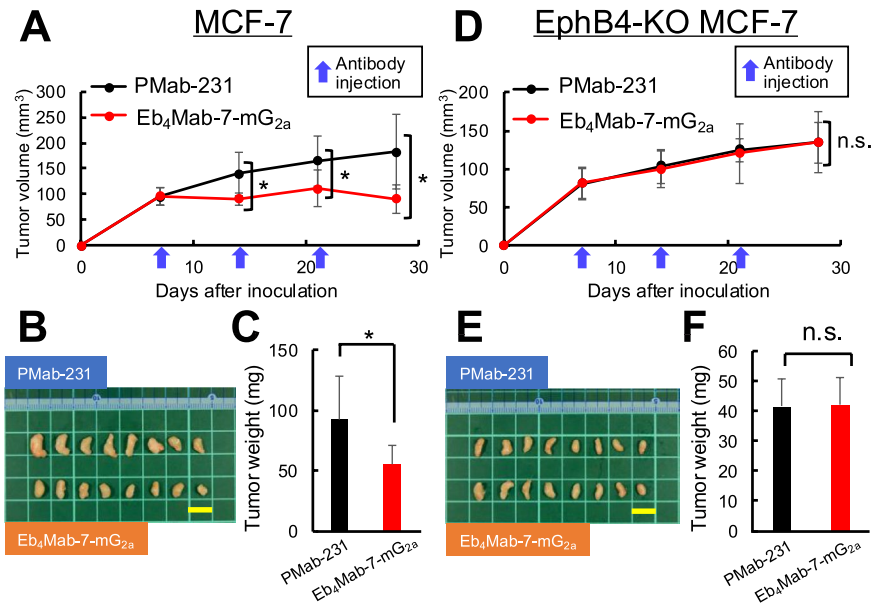

FIGURE 6 | Antitumor activity of $Eb_4Mab\text{-}7\text{-}mG_{2a}$ against MCF-7 and EphB4-KO MCF-7 tumors in vivo. MCF-7 and EphB4-KO MCF-7 cells were subcutaneously inoculated into BALB/c nude mice on Day 0. $Eb_4Mab\text{-}7\text{-}mG_{2a}$ (100 μg) or the control antibody PMab-231 (100 μg) was administered intraperitoneally on Days 7, 14, and 21 (indicated by blue arrows). (A, D) Tumor growth curves of MCF-7 (A) and EphB4-KO MCF-7 (D) xenografts. Tumor volumes are presented as mean ± SD. *$p < 0.05$ (two-way ANOVA with Sidak's multiple comparisons test). (B, E) Representative images of resected tumors derived from MCF-7 (B) and EphB4-KO MCF-7 (E) xenografts (scale bar: 1 cm). (C, F) Tumor weights at the endpoint from MCF-7 (C) and EphB4-KO MCF-7 (F) xenografts. *$p < 0.05$ (two-way ANOVA with Sidak's multiple comparisons test).

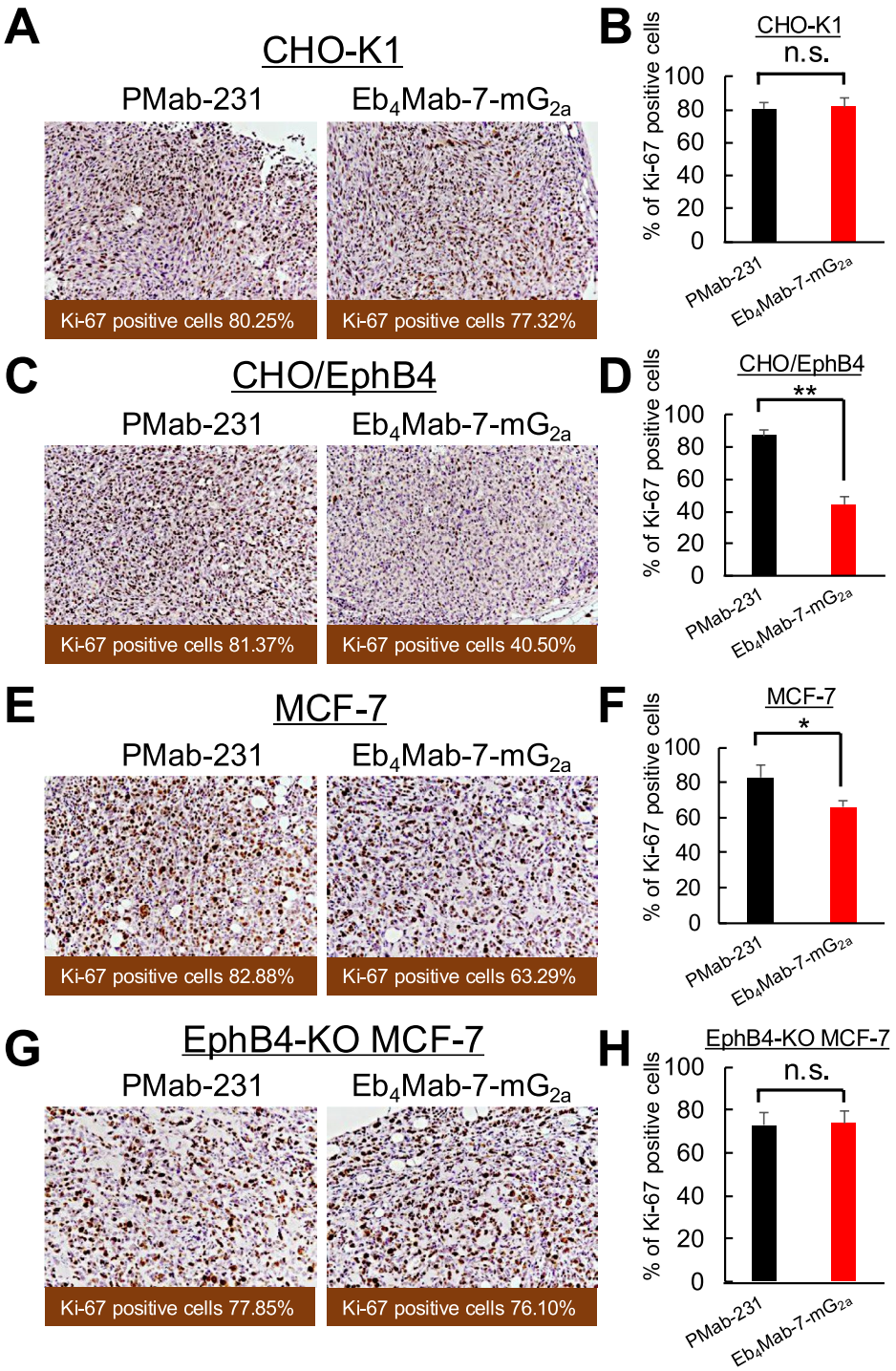

FIGURE 7 | $Eb_4Mab\text{-}7\text{-}mG_{2a}$-induced inhibition of tumor cell proliferation measured using Ki-67 staining. Xenograft sections derived from CHO-K1, CHO/EphB4, MCF-7, and EphB4-KO MCF-7 were immunohistochemically stained with anti-Ki-67 antibody to assess cell proliferation. Representative Ki-67 staining images (left panels) and quantification of Ki-67-positive cells (right panels) are presented for each group. Mice were treated with $Eb_4Mab\text{-}7\text{-}mG_{2a}$ or the control PMab-231. e-Path image analysis software was used to calculate the percentage of Ki-67-positive cells, which is presented as mean ± SD shown in the positive direction only. $^*p < 0.05$, $^{**}p < 0.01$ (one-way ANOVA with Tukey's multiple comparisons test). n.s., not significant.

cytotoxic T cell function, as well as by variable levels of complement and immunomodulatory cytokines [21]. The efficacy of Fc-mediated cytotoxicity is thus likely to depend on TME characteristics such as the density and activation status of effector immune cells (e.g., NK cells and macrophages) and the availability of complement factors, as well as the expression of inhibitory receptors and cytokines [22]. Future studies employing syngeneic or humanized mouse models with well-characterized immune landscapes will be essential to validate the therapeutic relevance of ADCC/CDC in vivo and to determine which TME contexts are most permissive for effective immune-mediated antitumor activity [23].

Xenograft models were used to confirm the in vivo efficacy of Eb_4Mab-7-mG_{2a}. Notably, our findings showed that it significantly suppressed tumor growth and reduced Ki-67 positivity in EphB4-expressing tumors, without affecting EphB4-negative or EphB4-KO tumors (Figures 5–7). These results indicate that EphB4 expression is required for the antitumor effects of the antibody in this xenograft setting, independent of exogenous ephrin-B2 stimulation, and suggest that the treatment selectively targets EphB4-positive tumors without any detectable adverse effects in vivo.

Notably, our Western blot analysis demonstrated that EphB4 expression is barely detectable in both normal human breast tissue and the non-tumorigenic mammary epithelial cell line MCF10A (Figure 1C). Correspondingly, Eb_4Mab-7-mG_{2a} did not affect the proliferation of MCF10A cells, indicating no direct cytotoxicity in this non-tumorigenic mammary epithelial cell line (Figure S1A). The antibody also had no effect on the proliferation of EphB4-positive MCF-7 or HBC5 breast cancer cells in the absence of immune effectors or ligand stimulation (Figure S1B,C). Consistent with these in vitro findings, the antibody exerted significant antitumor effects only in EphB4-expressing xenografts in vivo, while no efficacy was observed in EphB4-negative CHO-K1 or EphB4-KO MCF-7 xenografts (Figures 5–7). Moreover, no signs of systemic toxicity, including significant body weight loss, were detected in any treatment group (Figures 5–7 and Figures S2 and S3), suggesting EphB4-specific activity and supporting its favorable safety profile in vivo.

Humanization of the antibody backbone will be essential to reduce immunogenicity and improve pharmacokinetic properties in humans. Although EphB4 is preferentially expressed in tumors, its basal expression in some normal tissues remains a concern about potential antigen-dependent toxicity in normal tissues. Indeed, our Western blot analysis revealed that EphB4 is barely detectable in normal human breast tissue and non-tumorigenic mammary epithelial MCF10A cells (Figure 1C), consistent with previous reports demonstrating tumor-specific upregulation of EphB4 [18, 19, 24]. To further mitigate this target-related adverse effect outside tumors, reengineering Eb_4Mab-7-mG_{2a} into a cancer-specific monoclonal antibody (CasMab) format may improve tumor selectivity by recognizing glycoforms or conformational epitopes uniquely presented in tumor cells [25]. This approach has been successfully applied to PDPN-targeting antibodies and may be adapted for EphB4-targeted therapeutics [26, 27]. In parallel, additional strategies such as affinity tuning or bispecific antibody formats could enhance tumor specificity while sparing normal tissues [28, 29]. Finally, rigorous preclinical safety evaluation in non-human primates and humanized mouse models will be critical for advancing this antibody toward clinical development.

Clinical studies targeting the EphB4–Ephrin-B2 axis in combination with immune checkpoint inhibitors have shown promising results. In particular, soluble EphB4-human serum albumin (sEphB4-HSA) combined with pembrolizumab yielded response rates of 45% and 52% in human papillomavirus-negative head and neck squamous cell carcinoma and Ephrin-B2-positive urothelial carcinoma, respectively [30, 31]. In contrast, one study found that monotherapy with EphB4 blockade had no significant impact on metastatic castration-resistant prostate cancer [32], highlighting the importance of tumor context and therapeutic design. Unlike soluble receptor traps, Eb_4Mab-7-mG_{2a} offers dual action through both ligand blockade (Figure 2) and immune engagement (Figure 4), which may enable single-agent efficacy or synergize with existing immunotherapies.

Future studies should therefore explore the therapeutic potential of Eb_4Mab-7-mG_{2a} in other EphB4-overexpressing malignancies, including those in which EphB4 plays a functional role in tumor progression and/or immune modulation. Given the observed context dependence of EphB4 signaling, careful selection of cancer types and companion biomarkers, such as Ephrin-B2 expression or downstream ERK activity, will be crucial for identifying responsive tumors. Apart from its potential as a monotherapy, Eb_4Mab-7-mG_{2a} may be particularly effective in combination with immune checkpoint inhibitors based on clinical studies showing synergy between EphB4 blockade and pembrolizumab across multiple tumor types [30, 31]. Comprehensive in vivo validation of combination regimens, together with detailed immune microenvironment profiling, will likely support the design and development of evidence-based therapies.

Beyond immune checkpoint inhibitors, other combination strategies may also enhance the efficacy of Eb_4Mab-7-mG_{2a}. Since EphB4 activation has been shown to stimulate the ERK signaling pathway both in our current study using EphB4-positive MCF-7 cells (Figure 2C) and in previous reports involving Ephrin-B2 stimulation or agonistic antibodies in the same MCF-7 cell line [8], combination with MEK inhibitors could provide synergistic suppression of tumor growth. Additionally, given the role of EphB4 in tumor angiogenesis and vascular remodeling [5], combining Eb_4Mab-7-mG_{2a} with anti-angiogenic agents such as vascular endothelial growth factor inhibitors may further potentiate antitumor effects. Rational design of such combination therapies, based on tumor molecular profiling, could expand the clinical applicability of Eb_4Mab-7-mG_{2a}.

To facilitate clinical translation, further optimization of Eb_4Mab-7-mG_{2a}—including antibody humanization and preclinical safety evaluation in relevant models—is warranted. Additional strategies such as affinity tuning, bispecific formats, or tumor-specific epitope targeting may enhance selectivity and minimize off-tumor effects. Additionally, the antigen recognition domain of Eb_4Mab-7-mG_{2a} could be incorporated into chimeric antigen receptor (CAR) T cells to expand its utility to cell-based immunotherapy. This modular strategy may be particularly valuable in solid tumors wherein tumor-specific antigens are limited and off-tumor toxicity remains a major concern [33]. Together, these findings suggest the need for continued development of Eb_4Mab-7-mG_{2a} across multiple modalities given its versatility and potential for precision oncology.

Author Contributions

Tomokazu Ohishi: funding acquisition, investigation, methodology, writing – original draft. **Hiroyuki Suzuki:** conceptualization, data curation, investigation. **Mika K. Kaneko:** conceptualization, data curation, investigation. **Tomohiro Tanaka:** conceptualization, data curation, funding acquisition, investigation. **Akiko Harakawa:** data

curation, investigation. **Junjiro Yoshida:** validation, visualization. **Daisuke Tatsuda:** validation, visualization. **Yukinari Kato:** conceptualization, funding acquisition, project administration, resources, writing – review and editing. **Manabu Kawada:** supervision.

Acknowledgments

The authors thank Shun-ichi Ohba, Kyohei Kurosawa, Hiroyuki Inoue, Hayamitsu Adachi, Isao Momose, Yoko Yamazaki, Shuichi Sakamoto, Takefumi Onodera, and Nana Hashimoto (Institute of Microbial Chemistry [BIKAKEN], Numazu, Microbial Chemistry Research Foundation) for their technical assistance and valuable experimental advice.

Disclosure

The authors declare no conflicts of interest.

Ethics Statement

Animal experiments were conducted in accordance with institutional guidelines and were approved by the Animal Ethics Committee of the Institute of Microbial Chemistry (approval no. 2024-071).

Consent

The authors have nothing to report.

Conflicts of Interest

The authors declare no conflicts of interest.

References

1. H. Sung, J. Ferlay, R. L. Siegel, et al., "Global Cancer Statistics 2020: GLOBOCAN Estimates of Incidence and Mortality Worldwide for 36 Cancers in 185 Countries," *CA: A Cancer Journal for Clinicians* 71 (2021): 209–249.

2. R. L. Siegel, K. D. Miller, H. E. Fuchs, and A. Jemal, "Cancer Statistics, 2022," *CA: A Cancer Journal for Clinicians* 72 (2022): 7–33.

3. E. B. Pasquale, "Eph Receptor Signalling Casts a Wide Net on Cell Behaviour," *Nature Reviews. Molecular Cell Biology* 6 (2005): 462–475.

4. E. B. Pasquale, "Eph-Ephrin Bidirectional Signaling in Physiology and Disease," *Cell* 133 (2008): 38–52.

5. E. B. Pasquale, "Eph Receptors and Ephrins in Cancer: Bidirectional Signalling and Beyond," *Nature Reviews. Cancer* 10 (2010): 165–180.

6. N. K. Noren, G. Foos, C. A. Hauser, and E. B. Pasquale, "The EphB4 Receptor Suppresses Breast Cancer Cell Tumorigenicity Through an Abl-Crk Pathway," *Nature Cell Biology* 8 (2006): 815–825.

7. A. Barquilla and E. B. Pasquale, "Eph Receptors and Ephrins: Therapeutic Opportunities," *Annual Review of Pharmacology and Toxicology* 55 (2015): 465–487.

8. Z. Xiao, R. Carrasco, K. Kinneer, et al., "EphB4 Promotes or Suppresses Ras/MEK/ERK Pathway in a Context-Dependent Manner: Implications for EphB4 as a Cancer Target," *Cancer Biology & Therapy* 13 (2012): 630–637.

9. G. Martiny-Baron, T. Korff, F. Schaffner, et al., "Inhibition of Tumor Growth and Angiogenesis by Soluble EphB4," *Neoplasia* 6 (2004): 248–257.

10. R. Nanamiya, H. Suzuki, M. K. Kaneko, and Y. Kato, "Development of an Anti-EphB4 Monoclonal Antibody for Multiple Applications Against Breast Cancers," *Monoclonal Antibodies in Immunodiagnosis and Immunotherapy* 42 (2023): 166–177.

11. T. Manso, A. Kushwaha, N. Abdollahi, P. Duroux, V. Giudicelli, and S. Kossida, "Mechanisms of Action of Monoclonal Antibodies in Oncology Integrated in IMGT/mAb-DB," *Frontiers in Immunology* 14 (2023): 1129323.

12. C. Rodriguez-Nava, C. Ortuno-Pineda, B. Illades-Aguiar, et al., "Mechanisms of Action and Limitations of Monoclonal Antibodies and Single Chain Fragment Variable (scFv) in the Treatment of Cancer," *Biomedicine* 11 (2023): 11.

13. H. Suzuki, T. Ohishi, T. Tanaka, M. K. Kaneko, and Y. Kato, "A Cancer-Specific Monoclonal Antibody Against Podocalyxin Exerted Antitumor Activities in Pancreatic Cancer Xenografts," *International Journal of Molecular Sciences* 25 (2023): 161.

14. T. Ohishi, T. Masuda, H. Abe, et al., "Monotherapy With a Novel Intervenolin Derivative, AS-1934, Is an Effective Treatment for *Helicobacter pylori* Infection," *Helicobacter* 23 (2018): e12470.

15. M. K. Kaneko, H. Suzuki, T. Ohishi, T. Nakamura, T. Tanaka, and Y. Kato, "A Cancer-Specific Monoclonal Antibody Against HER2 Exerts Antitumor Activities in Human Breast Cancer Xenograft Models," *International Journal of Molecular Sciences* 25 (2024): 1941.

16. M. Kawada, H. Inoue, M. Kajikawa, et al., "A Novel Monoclonal Antibody Targeting Coxsackie Virus and Adenovirus Receptor Inhibits Tumor Growth In Vivo," *Scientific Reports* 7 (2017): 40400.

17. S. R. Kumar, J. Singh, G. Xia, et al., "Receptor Tyrosine Kinase EphB4 Is a Survival Factor in Breast Cancer," *American Journal of Pathology* 169 (2006): 279–293.

18. J. Ding, Y. Yao, G. Huang, et al., "Targeting the EphB4 Receptor Tyrosine Kinase Sensitizes HER2-Positive Breast Cancer Cells to Lapatinib," *Cancer Letters* 475 (2020): 53–64.

19. D. M. Brantley-Sieders, A. Jiang, K. Sarma, et al., "Eph/Ephrin Profiling in Human Breast Cancer Reveals Significant Associations Between Expression Level and Clinical Outcome," *PLoS One* 6 (2011): e24426.

20. W. H. Fridman, F. Pages, C. Sautes-Fridman, and J. Galon, "The Immune Contexture in Human Tumours: Impact on Clinical Outcome," *Nature Reviews. Cancer* 12 (2012): 298–306.

21. M. Binnewies, E. W. Roberts, K. Kersten, et al., "Understanding the Tumor Immune Microenvironment (TIME) for Effective Therapy," *Nature Medicine* 24 (2018): 541–550.

22. C. Lo Nigro, M. Macagno, D. Sangiolo, L. Bertolaccini, M. Aglietta, and M. C. Merlano, "NK-Mediated Antibody-Dependent Cell-Mediated Cytotoxicity in Solid Tumors: Biological Evidence and Clinical Perspectives," *Annals of Translational Medicine* 7 (2019): 105.

23. M. Kishore, K. C. P. Cheung, H. Fu, et al., "Regulatory T Cell Migration Is Dependent on Glucokinase-Mediated Glycolysis," *Immunity* 48 (2018): 831–832.

24. S. R. Kumar, R. Masood, W. A. Spannuth, et al., "The Receptor Tyrosine Kinase EphB4 Is Overexpressed in Ovarian Cancer, Provides Survival Signals and Predicts Poor Outcome," *British Journal of Cancer* 96 (2007): 1083–1091.

25. Y. Kato and M. K. Kaneko, "A Cancer-Specific Monoclonal Antibody Recognizes the Aberrantly Glycosylated Podoplanin," *Scientific Reports* 4 (2014): 5924.

26. L. Chalise, A. Kato, M. Ohno, et al., "Efficacy of Cancer-Specific Anti-Podoplanin CAR-T Cells and Oncolytic Herpes Virus G47Delta Combination Therapy Against Glioblastoma," *Molecular Therapy - Oncolytics* 26 (2022): 265–274.

27. T. Tanaka, H. Suzuki, T. Ohishi, M. K. Kaneko, and Y. Kato, "A Cancer-Specific Anti-Podoplanin Monoclonal Antibody, PMab-117-mG(2a) Exerts Antitumor Activities in Human Tumor Xenograft Models," *Cells* 13 (2024): 1833.

28. R. E. Kontermann, "Dual Targeting Strategies With Bispecific Antibodies," *MAbs* 4 (2012): 182–197.

29. E. R. Vander Mause, D. Atanackovic, C. S. Lim, and T. Luetkens, "Roadmap to Affinity-Tuned Antibodies for Enhanced Chimeric Antigen Receptor T Cell Function and Selectivity," *Trends in Biotechnology* 40 (2022): 875–890.

30. A. Jackovich, B. J. Gitlitz, J. W. W. Tiu-Lim, et al., "Improved Efficacy of Pembrolizumab Combined With Soluble EphB4-Albumin in HPV-Negative EphrinB2 Positive Head Neck Squamous Cell Carcinoma," *Oncotarget* 15 (2024): 444–458.

31. S. Sadeghi, D. Quinn, T. Dorff, et al., "EphrinB2 Inhibition and Pembrolizumab in Metastatic Urothelial Carcinoma," *Journal of Clinical Oncology* 41 (2023): 640–650.

32. D. J. Vander Weele, M. Kocherginsky, S. Munir, et al., "A Phase II Study of sEphB4-HSA in Metastatic Castration-Resistant Prostate Cancer," *Clinical Genitourinary Cancer* 20 (2022): 575–580.

33. A. J. Hou, L. C. Chen, and Y. Y. Chen, "Navigating CAR-T Cells Through the Solid-Tumour Microenvironment," *Nature Reviews. Drug Discovery* 20 (2021): 531–550.

Supporting Information

Additional supporting information can be found online in the Supporting Information section. **Figure S1:** Eb_4Mab-7-mG_{2a} alone does not affect cell proliferation. (A–C) Cell viability of MCF10A (A), MCF-7 (B), and HBC5 (C) cells treated with either control PMab-231 or Eb_4Mab-7-mG_{2a} at 5 μg/mL for 0–3 days. Cell viability was assessed using the MTS assay and normalized to Day 0 (set as 1.0). No significant differences in any of the cell lines tested (n.s.) were observed between the two groups. Data are presented as mean ± SD of triplicate experiments. **Figure S2:** Supplementary data for Figure 5. (A) Body weights of mice bearing CHO-K1 xenografts presented as mean ± SD. n.s., not significant (two-way ANOVA with Sidak's multiple comparisons test) (left), and images of mice bearing CHO-K1 xenografts before resection (right). (B) Body weights of mice bearing CHO/EphB4 xenografts presented as mean ± SD. n.s., not significant (two-way ANOVA with Sidak's multiple comparisons test) (left), and images of mice bearing CHO/EphB4 xenografts before resection (right). **Figure S3:** Supplementary data for Figure 6. (A) Body weights of mice bearing MCF-7 tumors presented as mean ± SD. n.s., not significant (two-way ANOVA with Sidak's multiple comparisons test) (left), and images of mice bearing MCF-7 tumors before tumor resection (right). (B) Body weights of mice bearing EphB4-KO MCF-7 tumors presented as mean ± SD. n.s., not significant (two-way ANOVA with Sidak's multiple comparisons test) (left), and images of mice bearing EphB4-KO MCF-7 tumors before tumor resection (right). **Table S1:** Kaplan–Meier survival analysis summary for EphB family genes in breast cancer.